Gate-Optimized rGO-Flake-Based Field-Effect Transistor for Selective Detection of Nitrogen in Soil for Precision Farming

Nimisha; Sett, Avik; Tewari, Virendra Kumar; Bhattacharyya, Tarun Kanti

DOI
10.1109/JSEN.2025.3565148

Publication date
2025

Document Version
Final published version

Published in
IEEE Sensors Journal

Gate-Optimized rGO-Flake-Based Field-Effect Transistor for Selective Detection of Nitrogen in Soil for Precision Farming

Nimisha, Avik Sett, Virendra Kumar Tewari, and Tarun Kanti Bhattacharyya

***Abstract*—The inadequate use of fertilizer leads to an imbalance of nitrogen in soil, which presents significant challenges to sustainable agriculture. To address this issue, a novel soil nitrogen sensor using reduced graphene oxide (rGO)-based field-effect transistor (FET) is proposed. In soil, nitrogen is present in the form of nitrate, nitrite, and ammonium ion; however, as nitrite content is exceptionally low, the detection of nitrite is not possible. Most of the research focuses on nitrate detection, but simultaneous detection of nitrate and ammonium ions is highly significant and challenging. The proposed concept enables a single FET device to detect both ammonium and nitrate ions at different gate potentials. The sensor demonstrates a very high response of 1050% for 3.5-ppm nitrate ion with a sensitivity of 0.9 μA/ppm and 860% for 3.5-ppm ammonium ion with a sensitivity of 0.45 μA/ppm at an optimized V_{gs} of 3.9 and 0.8 V, respectively. Moreover, the sensor exhibits promising attributes, including high selectivity and rapid response (35 s for NO_3^- ions and 41 s for NH_4^+ ions). This facilitates real-time monitoring of soil nitrogen levels for precision agriculture applications.**

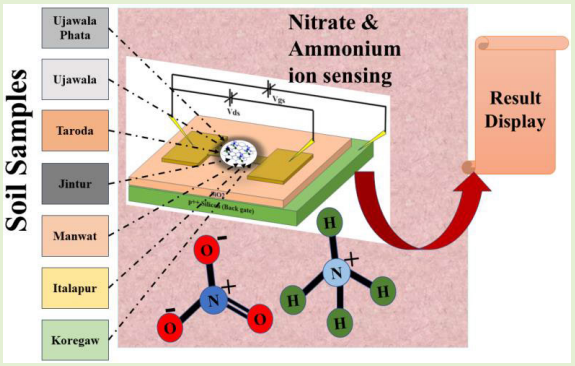

***Index Terms*— Field-effect transistor (FET), nitrogen sensor, reduced graphene oxide (rGO), selectivity, soil sensor.**

I. Introduction

INDIA is a nation dependent on agriculture. More than 80% of rural India's population is supported primarily by agriculture and its allied activities. Population growth is causing an increase in the global demand for agricultural products. According to the Food and Agriculture Organization of the United Nations, 70% more food will be required to be produced globally by 2050. The soil plays a crucial function in increasing crop production in agriculture. To increase crop yield, we need an adequate amount of fertilizers for the soil [1]. However, due to a dearth of technological knowledge, many farmers do not know the quantity of nutrients present in the soil and the additional quantity required for the appropriate growth of crops. Consequently, measuring the quantity of nutrients has become a formidable obstacle. Soil is a heterogeneous mixture of different components since this cross-sensitivity is the major issue during the nutrient measurement. Soil memory refers to the properties retained by soils overextended periods. Soil moment refers to soil properties that change swiftly over hours and days. Pollutants persist in the soil significantly longer than in the air and water, and their impact on the soil may be undetectable for a considerable period. Therefore, the nutrients required for plant growth and its presence in the soil are divided into two parts: macronutrients and micronutrients. Two additional groups of macronutrients include primary and secondary nutrients. Primary nutrients include nitrogen, phosphorus, and potassium, whereas secondary nutrients involve calcium, magnesium, and sulfur. Among all, nitrogen is a key element for plant growth. It is a component of chlorophyll, which imparts green color to plants. Photosynthesis occurs at high rates when a sufficient amount of nitrogen is present. It is also a beneficial element among all amino acids. Amino acids are building blocks for proteins. Plants require vast amounts of nitrogen. In plant tissue, nitrogen content varies from 1% to 6%. Therefore, nitrogen plays a very important role in plant growth. In soil,

Received 9 April 2025; accepted 23 April 2025. Date of publication 5 May 2025; date of current version 16 June 2025. The associate editor coordinating the review of this article and approving it for publication was Dr. Marios Sophocleous. *(Corresponding author: Tarun Kanti Bhattacharyya.)*

Nimisha and Tarun Kanti Bhattacharyya are with the Department of Electronics and Electrical Communication Engineering, IIT Kharagpur, Kharagpur 721302, India (e-mail: nimishan3@gmail.com; tkb.ece@iitkgp.ac.in).

Avik Sett is with the Department of Microelectronics, Delft University of Technology, 2628 CD Delft, The Netherlands (e-mail: aviksett210291@gmail.com).

Virendra Kumar Tewari is with the Department of Agriculture and Food Engineering, IIT Kharagpur, Kharagpur 721302, India (e-mail: vktfb@agfe.iitkgp.ac.in).

This article has supplementary downloadable material available at https://doi.org/10.1109/JSEN.2025.3565148, provided by the authors.

Digital Object Identifier 10.1109/JSEN.2025.3565148

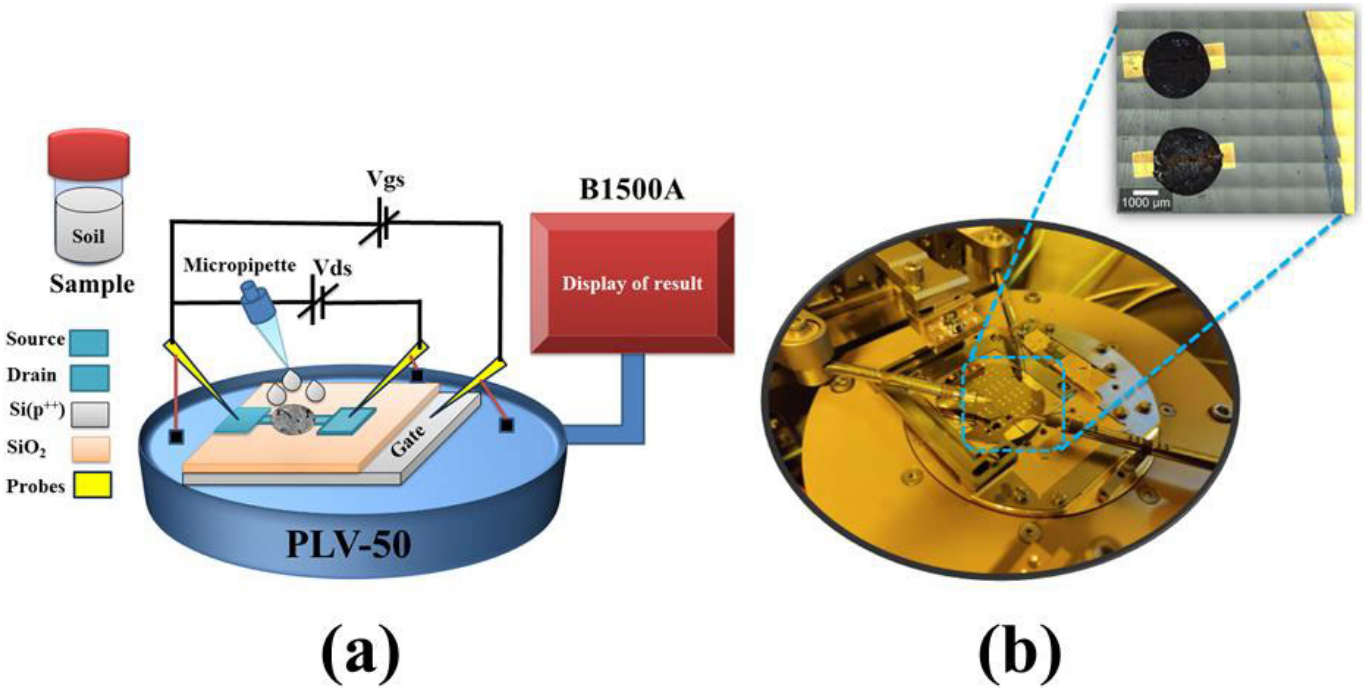

Fig. 1. (a) Schematic of the sensing device and setup. (b) Fabricated device structure.

nitrogen is present in the form of nitrate (NO_3^-), nitrite (NO_2^-), and ammonium (NH_4^+) ions. Nitrate and ammonium ions are present in detectable form, but nitrite content is very low and undetectable. Therefore, detection of available nitrogen is done by the total amount of NO_3^- and NH_4^+ ions present in the soil sample. There are various techniques to measure nitrogen content in the soil, which include optical spectroscopy, electrical conductivity (EC), resistivity, and permittivity (e.g., EC, time domain reflectometry (TDR), and frequency domain reflectometry (FDR) probe), passive radiometry (e.g., microwave and gamma ray), strength-based sensing [e.g., direct shear test (DST) and torsional shear test (TST)], and electrochemical method. However, all of these techniques are time-consuming and complex, and there is a huge chance of interference from other ions present in the soil sample [2], [3], [4], [5]. Moreover, previous reports emphasize either the detection of nitrate ions or ammonium ions. However, the presence of both ions contributes to the soil's total nitrogen content. Hence, a facile method to detect both ions simultaneously with high accuracy is the need of the hour.

Therefore, this research work aims to fabricate a novel FET-based soil sensor that can measure both nitrate and ammonium ions through tuning of gate potential. Functionalized reduced graphene oxide (rGO) is used as a sensing element, which assists in avoiding interference. The sensor shows the highest sensitivity at +3.9 V gate voltage for NO_3^- ions and 0.8 V gate voltage for NH_4^+ ions. Input gate voltage was swept from −10 to +10 V at a constant V_{ds} of +2 V. Soil is a heterogeneous mixture of various elements whose ionization potential differs for different elements. Therefore, when the gate voltage is swept from −10 to +10 V, every element exhibits maximum response at different gate voltages (NO_3^- at +3.9 V, NH_4^+ at 0.8 V, K^+ at −8.9 V, Ca^+ at −8.7 V, Cu^+ at −9.01 V, SO_4^- at 6 V, Mg^+ at −5.94 V, Cl^- at 7 V, Ni^+ at −9.1 V, and Zn^+ at −8.42 V). This technique shall reduce the interference from the various elements in the soil sample and accurately detect the soil's nitrogen content.

II. Sensor Fabrication and Material Characterization

A. Device Fabrication and Experimental Setup

The back-gate field-effect transistor is fabricated using a p⟨100⟩-type, heavily doped with boron, single-sided polished 2-in wafer (resistivity: −0.001 to 0.005 cm). Over silicon, a 200-nm thermal oxide (dry–wet–dry) was grown to produce insulation (SiO_2). The edge of the Si/SiO_2 wafer was masked with Kapton tape and spin-coated with positive photoresist at 3000 r/min for 20 s. The wafer is then baked for 20 min, the Kapton tape is removed, and the etching of the Si/SiO_2 wafer (40 min) is performed using BHF to create the back gate. A 100-nm Ti interlayer was deposited to enhance the adhesion of Au to SiO_2. The gold layer (300 nm in thickness) was deposited over the Ti layer via dc sputtering. The dc power was fixed at 70 W, and the deposition rates for Au and Ti were fixed at 2.4 Å/s and 0.5 Å/s, respectively. The Ti–Au layer was lithographically patterned to create the source, drain, and back gate. The fabricated device has a channel length of 30 μm and a channel width of 240 μm. The channel length is kept at 30 μm so that an appropriate amount of the soil sample can interact with the channel material, which is also responsible for higher operating voltage.

The lithographically patterned device shows the source, drain, and back gate with its sensing setup; its schematic is shown in Fig. 1(a) and the fabricated device image is shown in Fig. 1(b). PLV-50 probe station along with B-1500A semiconductor device parameter analyzer was used to evaluate the device performances.

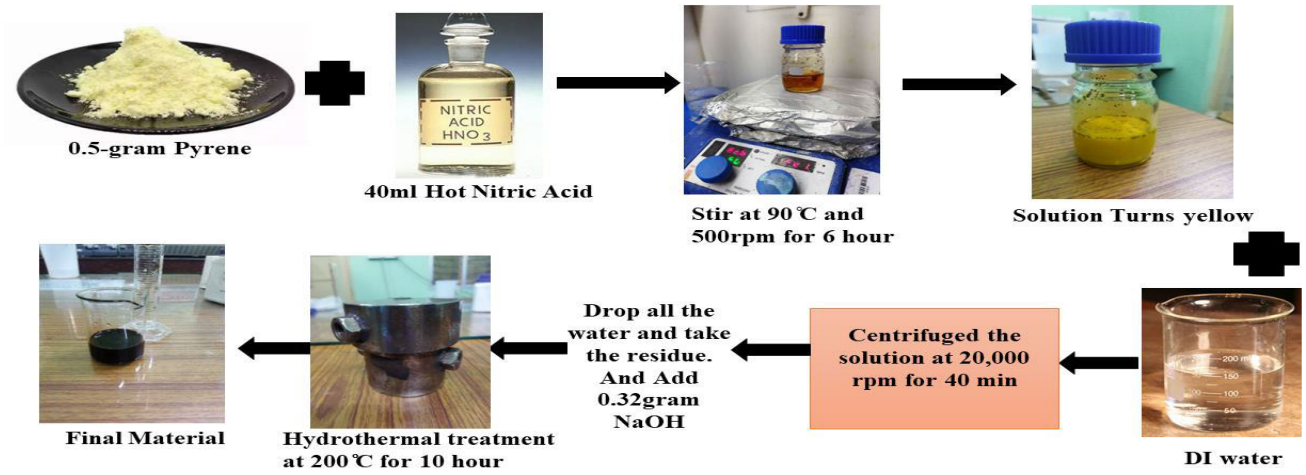

Fig. 2. Synthesis of rGO-flake sensing layer by pyrene.

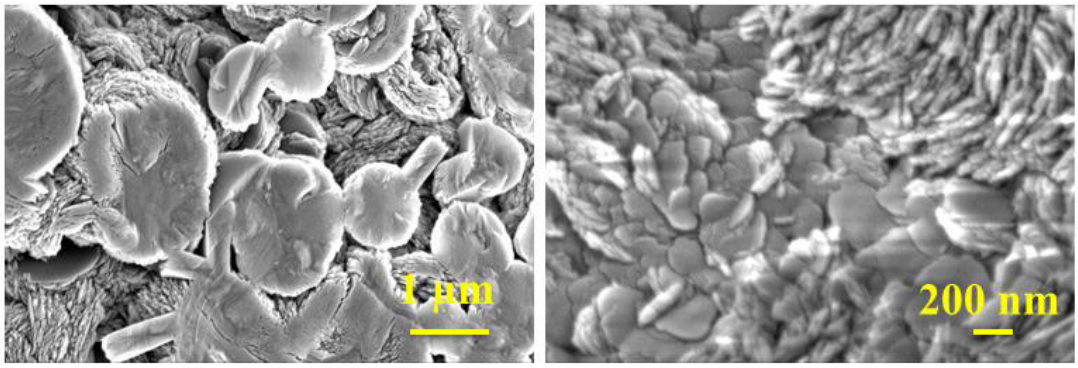

Fig. 3. Structural and morphological investigation of graphene-based nanostructured sensing layer; SEM image of rGO flakes.

B. Synthesis of the rGO-Flake Sheet

The oxygenated rGO flakes are synthesized by hydrothermal treatment of pyrene, as displayed in Fig. 2. Pyrene (0.5 g) was nitrated in hot nitric acid (40 ml) at 90 °C under stirring for 6 h at 500 r/min. The solution turns yellow in color. After removing the acid by washing it with deionized water (DI) water, the solution is centrifuged at 20 000 r/min for 40 min. The residue is collected from the previous process. Furthermore, 0.32 g of NaOH aqueous solution is added to the mixture, and the resulting solution is treated hydrothermally at 200 °C for 10 h. Finally, a dark brown-colored oxygenated rGO-flake solution was successfully prepared for nitrogen sensing application. The attained rGO from pyrene is denoted as rGOP. The entire synthesis procedure is demonstrated in Fig. 2.

C. Characterization of rGO-Flake Sheets

The structural and morphological study of the prepared rGOP was done using UV–Vis spectroscopy, Fourier transform infrared spectroscopy, Raman spectroscopy, and FESEM. Fig. 3 shows the FESEM image of rGO nanosheets, depicting a clear picture of its flake-like structure that facilitates the physisorption of the selective species.

Fig. 4(a) shows the UV–Vis spectroscopic analysis of the sensing material; four peaks were observed, i.e., at 211.91, 280, 315.94, and 484.4 nm. The peak at 211.91 nm is due to the π-to-π^* transition of C=C, and the peak at 351.94 nm

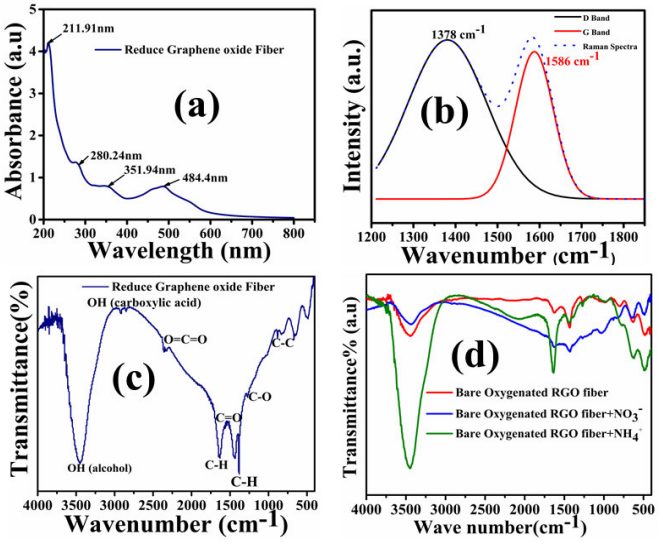

Fig. 4. (a) UV–Vis absorbance spectrum for rGO flakes, (b) Raman spectroscopy of rGO flakes, (c) FTIR spectra of rGO flakes, and (d) FTIR spectra of the interaction of NO^{3-} and NH^{4+} ions with prepared rGO flakes.

is attributed to the n-to-π^* transition of C–O. The peak at 280.24 nm is due to the n-to-π^* transition of C=O bonds [7]. The peak at 484.4 nm is due to the n-to-π^* transition of oxygen-containing groups and the presence of sp^2 domains due to the hydrothermal treatment of the material [8]. Fig. 4(b)

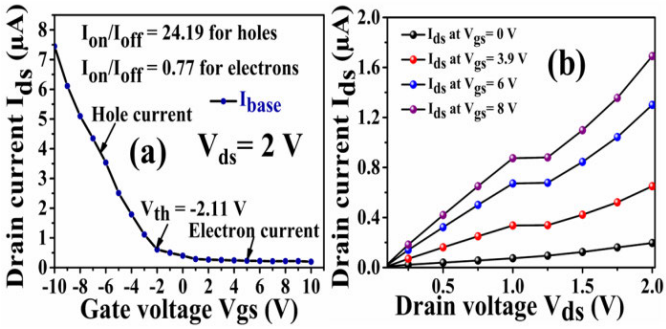

Fig. 5. (a) Transfer characteristics of the device. (b) Output characteristics of the device.

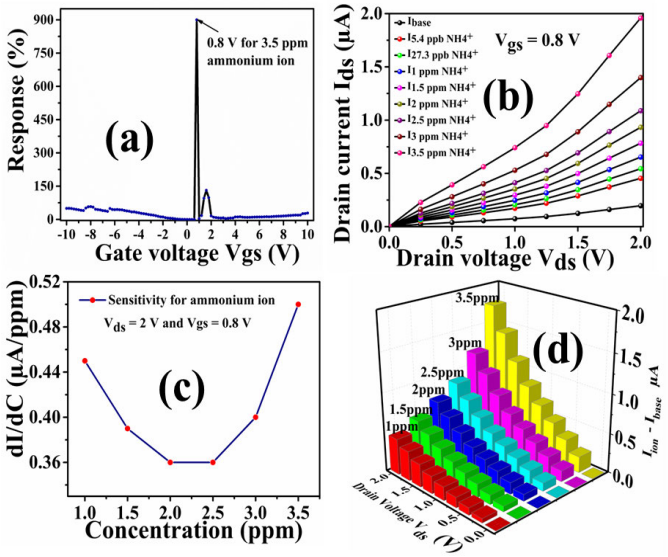

Fig. 6. (a) Gate voltage optimization of the device for ammonium ion. (b) I_{ds}–V_{ds} of FET device on absorbing NH_4^+ ions. (c) Sensitivity of the device for different concentrations of NH_4^+ ion. (d) Change in current due to variation in drain voltage and NH_4^+ ion concentration.

shows the Raman spectroscopic analysis of the prepared material. The D band at 1378 cm^{-1} and the G band at 1586 cm^{-1} are observed in the Raman plot. The I_D/I_G ratio is calculated to be 0.86, indicating a high percentage of defects created in the sensing material [7]. Fig. 4(c) shows the FTIR analysis of the sensing material. The presence of the OH group in the active sensing layer is responsible for NO_3^- ion adsorption. The other oxygen-containing groups, such as O=C=O, C=O, and C–O, are accountable for NH_4^+ ion adsorption. The FTIR spectrum in Fig. 4(d) depicts a clear interaction of the sensing material with NO_3^- and NH_4^+ ions at zero gate voltage. A shift in the wavenumber of the OH group from 3446 to 3434 cm^{-1} after the interaction of nitrate ions is observed. Furthermore, a shift in the wavenumber of the C=O group from 1431.03 to 1633.71 cm^{-1} is observed after interaction with ammonium ions.

III. Electrical Characterization

A. FET-Based Sensing Experimental Data Analysis

The electrical characteristics (I_{ds}–V_{gs}) for rGO field-effect transistor (FET) at $V_{ds} = 2$ V are shown in Fig. 5(a). The characteristics show that the material has excess holes compared to that of electrons. The Dirac point of the device is −2.11 V, indicating that the channel material is p-type. The transconductance of the device is calculated to be 7.2 mA/V. The I_{on}/I_{off} ratio is 24.19 for the holes and 0.77 for the electrons as the device is generally ON. The output characteristics (I_{ds}–V_{ds}) are shown in Fig. 5(b) at different gate voltages. As the gate voltage increases, channel resistance decreases, and the drain current is observed to increase.

The selectivity of the fabricated device is tested due to the presence of all the major interfering elements (NO_3^-, NH_4^+, K^+, Ca^{+2}, Cu^{+2}, SO_4^{-2}, Mg^{+2}, Cl^{-2}, Ni^{+2}, Zn^{+2}, and PO_3^-) in the soil. For the calibration of the sensor, standard salts are used first, and then, the sensors are tested on the soil sample. Standard test solutions with a concentration of 4 ppm are prepared and tested on the device by modulating the drain voltage between 0 and 2 V. Current is seen to increase in the presence of NH_4Cl, $Ca(NO_3)_2$, $CuSO_4$, and H_3PO_4 but decreases in the presence of KNO_3, $MgCl_2$, $NiCl_2$, and $Zn(NO_3)_2$. An increase in current indicates an increase in holes, while a decrease in current indicates an increase in electrons. rGO flakes reveal a p-type structure with an abundance of holes as charge carriers and electron deficiency. The results shown in figure S1 in Supplementary Information are observed based on measurements from the semiconductor parameter analyzer (B1500). Gate electrostatics study is shown in figure S2 (Supplementary Information), due to the presence of all major interfering ions present in the soil. The response of the sensor is calculated as follows:

$$R = (I_{ion} - I_{base})/I_{base} * 100 \quad (1)$$

where I_{ion} is the current flowing through the sensor after adsorption of the ions present in the soil and I_{base} is the baseline current of the sensor without any ions. The major problem with electrochemical sensors is interference among the various other ions present in the soil. To avoid this interference, field-effect transistors are utilized to detect the presence of all the significant elements in the soil sample. The gate voltage is swept from −10 to +10 V, keeping $V_{ds} = +2$ V. It is found that the sensor demonstrates maximum response toward different ions at different gate voltages, such as NO_3^- at +3.9 V, NH_4^+ at 0.8 V, K^+ at −8.9 V, Ca^+ at −8.7 V, Cu^+ at −9.01 V, SO_4^- at 6 V, Mg^+ at −5.94 V, Cl^- at 7 V, Ni^+ at −9.1 V, and Zn^+ at −8.42 V, as shown in Supplementary Information S2. The sensor demonstrates a maximum response of 860% for 3.5-ppm ammonium ions at a gate voltage of 0.8 V, as shown in Fig. 6(a). Fig. 6(b) shows the I–V characteristics curve of the sensor device exposed to the $NH4^+$ ion concentration ranging from 5.4 ppb to 3.5 ppm. The current is observed to increase from 180 nA to 1.95 μA. The sensor does not show any response below 5.4 ppb. Hence, the lower detection limit for $NH4^+$ ion can be considered as 5.4 ppb. As ammonium ion concentration in soil is in the ppm range, the sensor works appropriately for soil applications. Fig. 6(c) depicts the device sensitivity toward different concentrations of $NH4^+$ ions at 0.8 V gate bias. The device's sensitivity is calculated by evaluating the change in current with a change in the concentration. In a

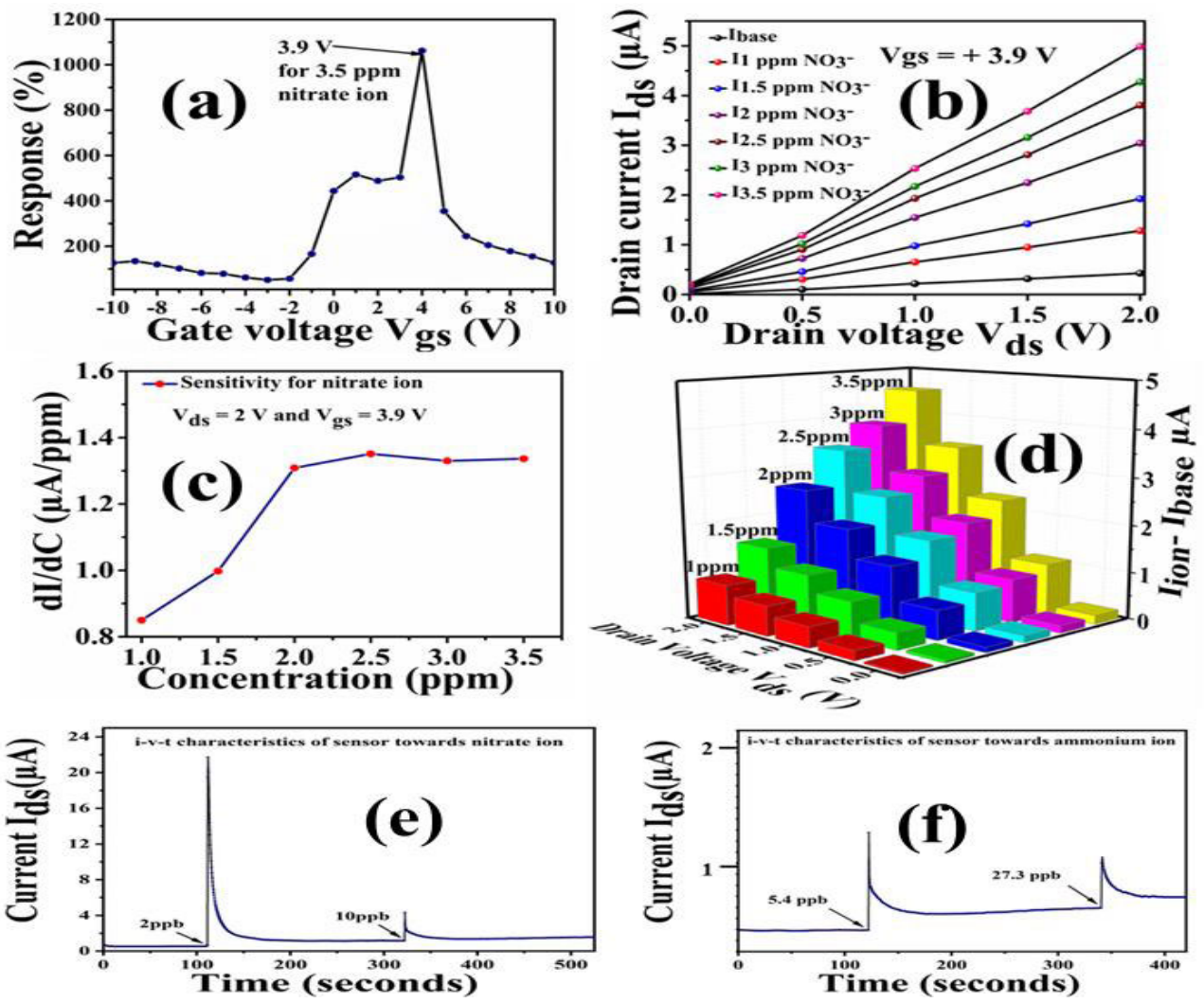

Fig. 7. (a) Response of the device for nitrate ion as a function of gate voltage. (b) I_{ds}–V_{ds} plot for nitrate ion detection at 3.9-V gate. (c) Sensitivity of the device for nitrate ion. (d) Change in current as a function of V_{ds} and nitrate ion concentration. (e) Transient response of the sensor for nitrate ion. (f) Transient response of the sensor for ammonium ion.

linear scale, the device's sensitivity is calculated for 1, 1.5, 2, 2.5, 3, and 3.5 ppm concentration. The sensor's sensitivity of 0.45 μA/ppm at 1 ppm reduces to 0.39 μA/ppm for 1.5 ppm and 0.36 μA/ppm for 2 ppm because of electrostatic repulsion of $NH4^+$ ions shown in Fig. 6(c). Beyond 2 ppm, the sensitivity increases as the concentration of ammonium ions increases. As the device acts as a soil nitrogen sensor and the concentration of nitrogen in soil is greater than 2 ppm, hence, nitrogen content in soil samples can be measured efficiently. Fig. 6(d) clearly shows the increase in current with an increase in concentration and voltage. The fabricated device is found to be highly sensitive to $NH4^+$ ions.

Fig. 7(a) shows that the maximum response of 1050% was obtained for nitrate ion at +3.9 V, which is very high due to the presence of the OH group. The OH group in the sensing layer has a partially positive charge on the hydrogen atom, which interacts with the NO_3^- ion, forming a hydrogen bond. For nitrate detection, the device was tuned at a gate voltage of +3.9 V. At +3.9 V, the concentration of electrons is minimal. The sensing response is defined as the ratio of the change in electron concentration to the original electron concentration in the channel. Fig. 7(b) shows the output characteristics (I_{ds}–V_{ds}) for the FET device at $V_{gs} = +3.9$ V.

At +3.9 V, electron concentration in the channel is minimized, which enhances the sensitivity of the device. Without any ions, the device exhibits 0.42 μA current, and when 1 ppm of NO_3^- ions (2-μL solution added by micropipette) is added onto the channel (20 min), the current increases to 1.2 μA. This is due to electron donation by the NO_3^- ions. With the further addition of NO_3^- ions, the current is observed to increase. The device's sensitivity is calculated by the change in current with respect to the change in concentration of target ions, as shown in Fig. 7(c). The sensitivity of the device is calculated at 1, 1.5, 2, 2.5, 3, and 3.5 ppm, and it is found that at 1 ppm, the device sensitivity is 0.9 μA/ppm. Sensitivity is observed to increase by increasing NO_3^- concentration at gate voltage $V_{gs} = +3.9$ V. Fig. 7(d) represents the change in drain current as a function of drain voltage and NO_3^- concentration.

Fig. 7(e) and (f) shows the transient response (i–v–t) of the FET sensor from 2 to 10 ppb for nitrate ion and 5.4–

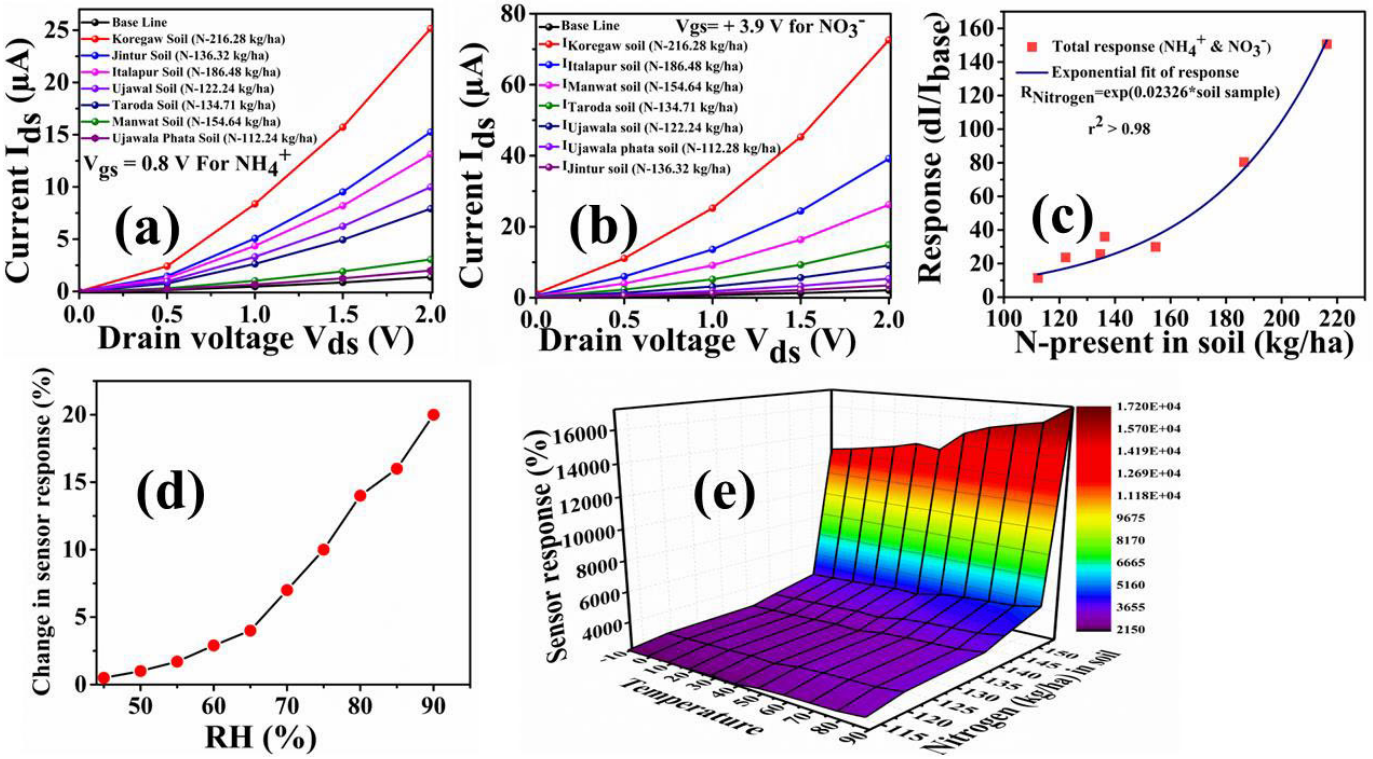

Fig. 8. (a) I_{ds}–V_{ds} of FET device on absorbing NH_4^+ ions of various soil samples. (b) I_{ds}–V_{ds} of FET device on absorbing NO_3^- ions of various soil samples. (c) Sensor response with respect to the nitrogen present in the soil. (d) Change in sensor response with RH (%). (e) Temperature effect on the sensor device.

27.3 ppb for ammonium ion, respectively. After immobilizing ions in the channel, spikes are observed, which are due to a change in resistance initiated by water molecules in the channel. However, with time, the ions get absorbed and the sensor reaches a new current level and becomes stable until further ions are drop-casted. The response time of the sensor is calculated to be 35 s for nitrate ions and 41 s for ammonium ions, which is excellent for portable nitrogen detection systems for soil.

The performance of the sensor on the soil sample, the stability of the sensor in varying humidity conditions, and the temperature effect are explained. Soil samples are collected from seven different locations of Maharashtra and nearby places, namely, Karegaon (N-216.28 kg/ha), Italapur (N-186.48 kg/ha), Manwat (N-154.64 kg/ha), Jintur (N-136.32 kg/ha), Taroda (N-134.71 kg/ha), Ujawala (N-122.24 kg/ha), and Ujawala Phata (N-112.28 kg/ha). The soil samples are prepared by taking 2.5 g of each soil and mixing it with 100 mL of DI water, after which the solution is ultrasonicated for 90 min. The solution is further centrifuged at 20 000 r/min for 15 min and collected as a fresh solution. On varying the gate voltage from −10 to +10 V, it is found that at 0.8 V gate potential, the sensor shows the maximum response for NH_4^+ ions, as shown in Fig. 8(a). The maximum response is achieved at +3.9 V gate potential for NO_3^- ions, as shown in Fig. 8(b). Available nitrogen is present in soil in the form of NO_3^- and NH_4^+, but the presence of NO_3^- is more predominant than NH_4^+. Therefore, when the soil sample is tested, it is found that the sensor responds more to NO_3^- ions than NH_4^+ ions. Fig. 8(c) shows the sensor response toward the total available nitrogen present in the soil sample, which is the sum of nitrate and ammonium response. Two different sensors fixed at 3.9 and 0.8-V gate were evaluated for nitrate and ammonium ions, respectively. The sum of the response from the two sensors was used to represent total nitrogen content as observed in Fig. 8(c). The details of the individual response are elaborated in Table S1 in Supplementary Information.

At a given concentration, the increase in RH % from 45 to 90 does not very much affect the sensing response of the soil nitrogen sensor. However, beyond 75% RH, there is a slight variation in the response, which means that the sensor's sensitivity is decreased, as shown in Fig. 8(d). The expected RH levels of fields encountered are less than 65%, which ensures that the fabricated sensor is humidity-tolerant. Fig. 8(e) shows the effect of temperature on sensor response. It is clearly visible that till 55 °C, the sensor response is fairly stable. After that, slight variations occur due to more electron–hole pair generation in the material. Temperature and humidity are the two critical parameters that affect the soil sensors. That is why this study plays a crucial role in soil sensor applications.

The repeatability and the response stability of the sensor are depicted in figure S4 (Supplementary Information). Five different sensors are tested for ammonium and nitrate ions to study the repeatability characteristics of the sensing layer. Table I shows the comprehensive comparison of soil nitrogen detection methods available in the literature. In this article, the gate-optimized FET sensing methodologies are professed

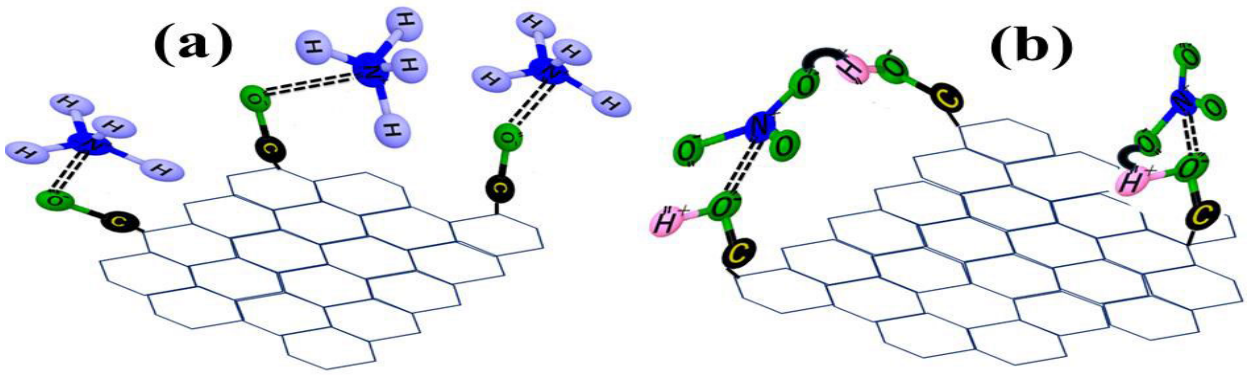

Fig. 9. (a) Sensing mechanism for NH_4^+. (b) Sensing mechanism for NO_3^-.

TABLE I
COMPREHENSIVE COMPARISON OF SOIL NITROGEN DETECTION METHODS

Detection method	Process Time	Detection Limit	Reference
Spectrophotometry	1-2 hour	0.5 -10 ppm	[13],[14],[15]
Visible-Near-Infrared Spectroscopy	2-3 hour	1 - 7 ppm	[16]
Mid-Infrared Spectroscopy	2- 3 hour	0.1 - 1 ppm	[17]
Raman Spectroscopy	2-3 hour	10-12 ppm	[18],[19]
Ion-Selective Electrode	4-5 minutes	0.2 ppm	[20],[21],[22], [23],[24]
Gate-Optimized FET	2 min	1 ppb	**[This work]**

to depict the lower process time and highly accurate detection limits of nitrate and ammonium ions in the soil. This engineered FET-based sensor is perfectly operable in the very low value of ions within the soil. The represented tabular data delineate the supremacy of the device, which will be a potential platform for precision farming in the near future.

B. Sensing Mechanism for Nitrate and Ammonium Ion

Reduced graphene oxide flakes consist of various functional groups, i.e., hydroxyl, carboxylic, and carbonyl [9], [10]. These functional groups are responsible for selective detection of nitrate and ammonium ions. For nitrate absorption, the OH group present in the graphene matrix plays a crucial role, as shown in Fig. 9(a). The partial negative charge present in the oxygen atom of the OH groups imparts a high affinity toward the positive N atom in the nitrate radicals [11]. The dangling oxygen atoms of the NO_3^- atoms may form bonds with the hydrogen atom of the hydroxyl group. Moreover, the carbonyl group is responsible for the absorption of ammonium ions [12], as shown in Fig. 9(b). The partial negative charge of the carbonyl group forms a bond with the ammonium ions, imparting the sensitive nature of the sensing material toward ammonium ions. This selective bond formation ensures nitrate and ammonium ion detection. The validation of sensing mechanism is shown in Fig. 4(d) of FTIR analysis where the wavenumber of the OH group is from 3446 to 3434 cm^{-1}, indicating the interaction of nitrate ions. Additionally, a notable shift in the wavenumber of the C=O group from 1431.03 to 1633.71 cm^{-1} is observed, suggesting interaction with ammonium ions.

IV. CONCLUSION

This research aims to develop a nitrogen soil sensor for precession agriculture. Due to soil heterogeneity, different detection methods are stated in the literature, but they all interfere. A peculiar FET-based design reduces interference by tailoring the gate voltage with all soil ions. A functional nitrogen soil sensor is built using this principle. Soil contains nitrate, nitrite, and ammonium ions. Since nitrite cannot be detected, ammonium and nitrate ions are studied. Hydrothermally treating pyrene yields rGO, which is drop casted over the FET device channel. Its channel length is 30 μm, and its threshold voltage is -2.4 V. The sensor's highest response for NO_3^- ions at $+3.9$ V is 1050%, and the sensor's highest response for NH_4^+ ions at 0.8 V is 860%, as shown by sweeping the gate voltage from -10 to $+10$ V. The other elements respond significantly low at varied gate voltages. A temperature and humidity study is also done, which shows that the sensor is almost independent of the humidity and temperature effect. Ammonium ions are detected at 5.4 ppb, while nitrate ions are at 1 ppb. The sensor's r^2 exceeds 0.98 on seven soil samples.

REFERENCES

[1] R. S. Velazquez-Gonzalez, A. L. Garcia-Garcia, E. Ventura-Zapata, J. D. O. Barceinas-Sanchez, and J. C. Sosa-Savedra, "A review on hydroponics and the technologies associated for medium- and small-scale operations," *Agriculture*, vol. 12, no. 5, p. 646, Apr. 2022.

[2] V. I. Adamchuk, E. D. Lund, B. Sethuramasamyraja, M. T. Morgan, A. Dobermann, and D. B. Marx, "Direct measurement of soil chemical properties on-the-go using ion-selective electrodes," *Comput. Electron. Agricult.*, vol. 48, no. 3, pp. 272–294, Sep. 2005, doi: 10.1016/j.compag.2005.05.001.

[3] V. I. Adamchuk, J. W. Hummel, M. T. Morgan, and S. K. Upadhyaya, "On-the-go soil sensors for precision agriculture," *Comput. Electron. Agricult.*, vol. 44, no. 1, pp. 71–91, Jul. 2004, doi: 10.1016/j.compag.2004.03.002.

[4] H. J. Kim, J. W. Hummel, and S. J. Birrell, "Evaluation of nitrate and potassium ion-selective membranes for soil macronutrient sensing," *Trans. ASABE*, vol. 49, no. 3, pp. 597–606, May 2006, doi: 10.13031/2013.20476.

[5] R. A. V. Rossel, V. I. Adamchuk, K. A. Sudduth, N. J. McKenzie, and C. Lobsey, "Proximal soil sensing: An effective approach for soil measurements in space and time," *Adv. Agronomy*, vol. 113, pp. 243–291, Jan. 2011, doi: 10.1016/b978-0-12-386473-4.00005-1.

[6] R. Chaudhary et al., "Fabrication and characterisation of Al gate n-metal–oxide–semiconductor field-effect transistor, on-chip fabricated with silicon nitride ion-sensitive field-effect transistor," *IET Comput. Digit. Techn.*, vol. 10, no. 5, pp. 268–272, Sep. 2016, doi: 10.1049/iet-cdt.2015.0174.

[7] S. Arunragsa, Y. Seekaew, W. Pon-On, and C. Wongchoosuk, "Hydroxyl edge-functionalized graphene quantum dots for gas-sensing applications," *Diamond Rel. Mater.*, vol. 105, May 2020, Art. no. 107790, doi: 10.1016/j.diamond.2020.107790.

[8] Z. Liu et al., "Size effect of graphene quantum dots on photoluminescence," *Molecules*, vol. 26, no. 13, p. 3922, Jun. 2021, doi: 10.3390/molecules26133922.

[9] D. Zaharie-Butucel, M. Potara, A. M. Craciun, R. Boukherroub, S. Szunerits, and S. Astilean, "Revealing the structure and functionality of graphene oxide and reduced graphene oxide/pyrene carboxylic acid interfaces by correlative spectral and imaging analysis," *Phys. Chem. Chem. Phys.*, vol. 19, no. 24, pp. 16038–16046, 2017, doi: 10.1039/c7cp02443f.

[10] M. Khan et al., "Pyrene functionalized highly reduced graphene oxide-palladium nanocomposite: A novel catalyst for the mizoroki-heck reaction in water," *Frontiers Chem.*, vol. 10, Apr. 2022, Art. no. 872366, doi: 10.3389/fchem.2022.872366.

[11] S. Tang and Z. Cao, "Adsorption of nitrogen oxides on graphene and graphene oxides: Insights from density functional calculations," *J. Chem. Phys.*, vol. 134, no. 4, Jan. 2011, Art. no. 044710, doi: 10.1063/1.3541249.

[12] B. Nozière, P. Dziedzic, and A. Córdova, "Products and kinetics of the liquid-phase reaction of glyoxal catalyzed by ammonium ions (NH_4^+)," *J. Phys. Chem. A*, vol. 113, no. 1, pp. 231–237, Jan. 2009, doi: 10.1021/jp8078293.

[13] K.-Y. Li et al., "Comparison of factors affecting soil nitrate nitrogen and ammonium nitrogen extraction," *Commun. Soil Sci. Plant Anal.*, vol. 43, no. 3, pp. 571–588, Feb. 2012, doi: 10.1080/00103624.2012.639108.

[14] R. A. Dorich and D. W. Nelson, "Direct colorimetric measurement of ammonium in potassium chloride extracts of soils," *Soil Sci. Soc. Amer. J.*, vol. 47, no. 4, pp. 833–836, Jul. 1983, doi: 10.2136/sssaj1983.03615995004700040042x.

[15] A. J. Kempers and A. Zweers, "Ammonium determination in soil extracts by the salicylate method," *Commun. Soil Sci. Plant Anal.*, vol. 17, no. 7, pp. 715–723, Jul. 1986, doi: 10.1080/00103628609367745.

[16] Z. Chen, S. Ren, R. Qin, and P. Nie, "Rapid detection of different types of soil nitrogen using near-infrared hyperspectral imaging," *Molecules*, vol. 27, no. 6, p. 2017, Mar. 2022, doi: 10.3390/molecules27062017.

[17] B. R. Jahn, R. Linker, S. K. Upadhyaya, A. Shaviv, D. C. Slaughter, and I. Shmulevich, "Mid-infrared spectroscopic determination of soil nitrate content," *Biosyst. Eng.*, vol. 94, no. 4, pp. 505–515, Aug. 2006, doi: 10.1016/j.biosystemseng.2006.05.011.

[18] R. Qin, Y. Zhang, S. Ren, and P. Nie, "Rapid detection of available nitrogen in soil by surface-enhanced Raman spectroscopy," *Int. J. Mol. Sci.*, vol. 23, no. 18, p. 10404, 2022, doi: 10.3390/ijms231810404.

[19] D. Diaz and D. W. Hahn, "Raman spectroscopy for detection of ammonium nitrate as an explosive precursor used in improvised explosive devices," *Spectrochimica Acta A, Mol. Biomolecular Spectrosc.*, vol. 233, Jun. 2020, Art. no. 118204, doi: 10.1016/j.saa.2020.118204.

[20] Y. Li, M. Zhang, J. Zheng, L. Pan, P. Kong, and Z. Lei, "Design and experiment of prototype soil pretreatment device for ISE-based soil nitrate-nitrogen detection," *Nongye Gongcheng Xuebao/Transactions Chin. Soc. Agricult. Eng.*, vol. 33, pp. 120–125, Feb. 2017, doi: 10.11975/j.issn.1002-6819.2017.z1.018.

[21] M. Zhang, M. Sheng, L. Zhang, L. Li, and Y. chao Zhang, "Development of soil available macronutrients detection system based on ion-selective electrodes array," *Nongye Jixie Xuebao/Transactions Chin. Soc. Agricult. Machinery*, vol. 43, pp. 277–282, Oct. 2012, doi: 10.6041/j.issn.1000-1298.2012.S0.057.

[22] G. Fiori, A. Betti, S. Bruzzone, P. D'Amico, and G. Iannaccone, "Nanodevices in Flatland: Two-dimensional graphene-based transistors with high I_{on}/I_{off} ratio," in *IEDM Tech. Dig.*, Dec. 2011, p. 11, doi: 10.1109/IEDM.2011.6131533.

[23] Y. Li, Q. Yang, M. Chen, M. Wang, and M. Zhang, "An ISE-based on-site soil nitrate nitrogen detection system," *Sensors*, vol. 19, no. 21, p. 4669, Oct. 2019. [Online]. Available: https://api.semanticscholar.org/CorpusID

[24] J. Choosang et al., "Simultaneous detection of ammonium and nitrate in environmental samples using on ion-selective electrode and comparison with portable colorimetric assays," *Sensors*, vol. 18, no. 10, p. 3555, Oct. 2018, doi: 10.3390/s18103555.

Nimisha is currently pursuing the Ph.D. degree with the Department of Electronics and Electrical Communication Engineering, Indian Institute of Technology, Kharagpur, India.

Her research interests include the fabrication of 2-D nanomaterial-based microsensors for soil and toxic metal ion sensing applications.

Avik Sett received the Ph.D. degree from the Department of Electronics and Electrical Communication Engineering, IIT Kharagpur, Kharagpur, India, in 2023.

He is currently serving as a Scientific Researcher at Delft University of Technology (TU Delft), Delft, The Netherlands. His current research deals with developing sensors for organ-on-chip applications.

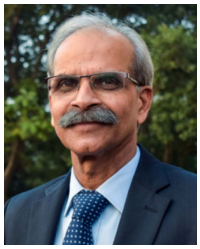

Virendra Kumar Tewari has been in the IIT system for the last 45 years from student to faculty. His field of specialization includes machinery systems design, industrial ergonomics and safety, and electronics and computer application in farm machinery design.

Tarun Kanti Bhattacharyya is currently a Professor and the HOD of the Department of Electronics and Electrical Communication Engineering, Indian Institute of Technology at Kharagpur, Kharagpur, India. His current research interests include low-power RF IC design, MEMS, and nanoelectronics.